17. F_1 Landsberg *qrt1*/Columbia *qrt1* plants were grown under 24-hour light in 1-inch (2.54-cm) square pots and treated with methanesulfonic acid ethyl ester (0.05%), 5-aza-2′-deoxycytidine (25 or 100 mg/liter), Zeocin (1 μg/ml), methanesulfonic acid methyl ester (75 parts per million), *cis*-diamminedichloroplatinum (20 μg/ml), mitomycin C (10 mg/liter), *N*-nitroso-*N*-ethylurea (100 μM), *n*-butyric acid (20 μM), trichostatin A (10 μM), or 3-methoxybenzamide (2 mM). Plants were watered and flower-bearing stems were immersed in these solutions. Alternatively, plants were exposed to 350-nm ultraviolet light (7 or 10 s) or heat shock (38° or 42°C for 2 hours). Pollen tetrads from these plants were used to pollinate Landsberg stigmas 3 to 5 days after each treatment; the F_1 plants were then subjected to additional treatments (up to five times per plant, every 3 to 5 days).
18. G. P. Copenhaver and C. S. Pikaard, *Plant J.* **9**, 259 (1996).
19. X. Sun, J. Wahlstrom, G. H. Karpen, *Cell* **91** 1007 (1997); E. B. Cambareri, R. Aisner, J. Carbon, *Mol. Cell. Biol.* **18**, 5465 (1998).
20. M. Bevan, I. Bancroft, H.-W. Mewes, R. Martienssen, R. McCombie, *Bioessays* **21**, 110 (1999).
21. R. M. Kuhn, L. Clarke, J. Carbon, *Proc. Natl. Acad. Sci. U.S.A.* **88**, 1306 (1991).
22. G. H. Karpen, *Curr. Opin. Genet. Dev.* **4**, 281 (1994); A. R. Lohe and A. J. Hilliker, *Curr. Opin. Genet. Dev.* **5**, 746 (1995).
23. H.-M. Li, K. Culligan, R. A. Dixon, J. Chory, *Plant Cell* **7**, 1599 (1995).
24. http://www.tigr.org/tdb/at/agad/.
25. U. Fleig, J. D. Beinhauer, J. H. Hegemann, *Nucleic Acids. Res.* **23**, 922 (1995).
26. G. P. Copenhaver and D. Preuss, *Curr. Opin. Plant Biol.* **2**, 104 (1999).
27. http://www.tigr.org/tdb/at/abe/bac_end_search.html.
28. C. J. Bell and J. R. Ecker, *Genomics* **19**, 137 (1994); A. Konieczny and F. M. Ausubel, *Plant J.* **4**, 403 (1993).
29. http://genome-www.stanford.edu/Arabidopsis/aboutcaps.html.
30. http://www.ncbi.nlm.nih.gov/Entrez/nucleotide.html; http://nucleus.cshl.org/protarab/AtRepBase.htm.
31. http://blast.wustl.edu.
32. B. Tugal, M. Pool, A. Baker, *Plant Physiol.* **120**, 309 (1999); J. F. Gutierrez-Marcos, M. A. Roberts, E. I. Campell, J. L. Wray, *Proc. Natl. Acad. Sci. U.S.A.* **93**, 13377 (1996); N. Inohara *et al.*, *J. Biol. Chem.* **266**, 7333 (1991); J. Callis, T. Carpenter, C-W. Sun, R. D. Vierstra, *Genetics* **139**, 921 (1995).
33. Supported in part by grants from the National Science Foundation, the U.S. Department of Agriculture, the Consortium for Plant Biotechnology Research, and the David and Lucile Packard Foundation. M.-I.B., S.K., X.L., M.B., G.M., B.H., L.D.P., W.R.M., R.A.M., and M.M. are members of the *Arabidopsis* Genome Initiative. We thank L. Mets, R. Esposito, S. Rounsley, J. A. Mayfield, and K. C. Keith for helpful discussions; R. Stein, D. Jurcin, P. Ridley, and E. Bent for technical assistance; and M. Spielman and S. Streatfeild for sharing genetic markers.

23 September; accepted 15 November 1999

Collisional Breakup in a Quantum System of Three Charged Particles

T. N. Rescigno,[1] M. Baertschy,[2] W. A. Isaacs,[3] C. W. McCurdy[2,3]

Since the invention of quantum mechanics, even the simplest example of the collisional breakup of a system of charged particles, $e^- + H \rightarrow H^+ + e^- + e^-$ (where e^- is an electron and H is hydrogen), has resisted solution and is now one of the last unsolved fundamental problems in atomic physics. A complete solution requires calculation of the energies and directions for a final state in which all three particles are moving away from each other. Even with supercomputers, the correct mathematical description of this state has proved difficult to apply. A framework for solving ionization problems in many areas of chemistry and physics is finally provided by a mathematical transformation of the Schrödinger equation that makes the final state tractable, providing the key to a numerical solution of this problem that reveals its full dynamics.

Electron-impact ionization of atoms and molecules is one of the most basic phenomena in low-energy collision physics. It is the fundamental mechanism for ion formation in mass spectroscopy and is responsible for forming and sustaining low-temperature plasmas that are used in applications ranging from fluorescent lighting to the processing of silicon chips. These collisions are governed by none of the selection rules that limit optical excitation, primarily because the incident electron cannot be distinguished from those of the target. Thus, electron impact stands as one of the most efficient means for exciting and ionizing atoms and molecules.

It seems almost incredible that even the simplest example of an electron impact–initiated breakup problem, the ionization of a hydrogen atom in a collision with an electron, has resisted solution until now. Although the Schrödinger equation has been known for more than 70 years, there has been no framework that allowed its complete solution for this case. In contrast, the bound states of the helium atom, another system with only two electrons, were computed accurately in the 1950s. That work established a framework that allowed the development of modern quantum chemistry as a practical discipline. The theoretical framework demonstrated here provides a basis for developing practical methods to treat ionizing collisions of electrons with atoms and molecules.

[1]Lawrence Livermore National Laboratory, Physics Directorate, Livermore, CA 94551, USA. [2]Department of Applied Science, University of California, Davis, Livermore, CA 94550, USA. [3]Lawrence Berkeley National Laboratory, Computing Sciences, Berkeley, CA 94720, USA.

The Quantum Mechanics of Three Charged Bodies

Although the analytic solution of the wave function for the isolated hydrogen atom played a pivotal role in establishing the new quantum theory during the early part of this century, no corresponding solutions exist for systems with three or more charged particles. Indeed, the nonrelativistic quantum mechanics of two-electron atoms has a long history, beginning with the work of Hylleraas (*1*) on bound states in the 1930s that culminated with Pekeris's (*2*) accurate determination of the bound states of helium in the late 1950s.

Scattering problems are intrinsically more difficult. It was not until 1961 that the simplest collision problem in a two-electron system, scattering of an electron by a hydrogen atom without energy exchange, was solved numerically by Schwartz (*3*) with Kohn's variational principle (*4*). Since then, the effort to solve the problem of collisions in which energy is transferred into excitation of states with quantum numbers n and l [$e^- + H(1s) \rightarrow e^- + H(nl)$] has produced benchmark calculations of excitation probabilities and angular distributions for excited bound states of the hydrogen atom. In the case in which only probabilities for excitation of the target atom are required, the traditional approach has been to expand the unknown solution of the Schrödinger equation in terms of the known wave functions of the target—the so-called "close-coupling" method. The initial applications of this method were confined to low energies at which only a few target states could be excited (*5*).

The next major hurdle to overcome was the extension of such studies to collision energies above that needed to ionize the target where a continuously infinite number of final states is possible. The convergence of the close-coupling method was convincingly and dramatically illustrated by Bray and Stelbovics (*6*) in 1993, who showed that a "convergent" close-coupling method could be developed for calculating elastic and excitation probabilities. They replaced the true ionized states of the hydrogen atom with a finite set of "pseudostates" and systematically increased their number until convergence was achieved. Using these ideas, they performed the first accurate computations of the total probability for ionization. Their work completed another chapter on the dynamics of two-electron systems, but not the final chapter. Attempts to use this approach to predict

any of the details of the process, such as the angular distributions for the two outgoing electrons or their respective energies, gave results that oscillate widely about the correct values (*7*) or require multiplication by unforeseeable overall constants to be comparable to experiment (*8*).

Although the first serious calculations on ionization by electron impact did not appear until the early 1990s, Peterkop (*9*) and simultaneously Rudge and Seaton (*10*) had worked out the mathematical theory of ionization in the early 1960s. The form of the wave function in which all three particles are widely separated places a boundary condition on the wave function that is so intractable that no known numerical approach to solving the Schrödinger equation has successfully incorporated it explicitly. The mathematical theory has given rise to a number of "ansatz" studies—a large number have appeared in recent years following the pioneering work of Brauner *et al.* (*11*) in 1989—in which aspects of the final state wave function for three charged particles are incorporated into an ad hoc formula for the ionization probability. A recent review of these calculations (*12*) has concluded that they perform poorly and that, in the few cases in which they appear to work well, the agreement with experiment is largely fortuitous. There is another promising approach that involves casting the problem in a time-dependent formulation (*13*), but it has not yet been applied to calculate the detailed ionization probabilities for the full problem of electron-impact ionization of hydrogen.

Only recently has the application of very large scale computing begun to yield results on this problem, unleashing a flurry of activity as the community began to see that a practical solution might be possible. Nevertheless, the complete breakup of a system of three charged particles has remained an unsolved problem until now. We found that an unambiguous numerical solution of this problem requires not only the kind of massively parallel computational resources that have only recently become available but also a fundamentally different approach to formulating the problem. This research article presents numerical results of calculations on electron-impact ionization of hydrogen by a method that can give complete details about the energy and angular distributions of the two outgoing electrons. The first calculations on the bound states of helium or on electron-impact excitation of the hydrogen atom opened the door to today's calculations on large molecules rich with previously unknown physical effects. Similarly, the complete calculations of electron-impact ionization of the hydrogen atom point the way to calculations on larger atoms and molecules that will unravel the more complicated dynamics of those ionizing collisions.

Quantum Scattering Wave Functions

In collision problems, in contrast to bound state problems, the wave functions are not localized but extend over all space. Collisions are intrinsically time-dependent, but the interactions depend only on distances and not explicitly on time, so the scattering information can be found by solving the time-independent Schrödinger equation familiar to both chemists and physicists:

$$H\Psi = E\Psi \qquad (1)$$

where H is the Hamiltonian operator, Ψ is the wave function, and E is total energy of the colliding system. When only one electron can escape to large distances from the nucleus, the form of the final state wave function is a product of a bound orbital for one electron (such as the 1s orbital of hydrogen) and a free wave [or more properly, an outgoing spherical wave, $\exp(ikr)/r$, where $i = \sqrt{-1}$, k is the momentum of the electron, and r is its distance from the nucleus] for the other. This is the boundary condition under which the Schrödinger equation is to be solved, and the wave function can be easily analyzed by matching to this known asymptotic form to give excitation probabilities and angular distributions.

For breakup collisions, the asymptotic form of the wave function is not so simple, and when the particles are charged, the situation is more complicated still. Two electrons can be at large distances from the nucleus, and one might expect the corresponding asymptotic form to be the product of the wave functions of two free electrons. However, because all three particles in this problem are charged, the Coulomb potentials between them fall off only as $1/r$, the reciprocal of the distances between them, which complicates the explicit form of the wave function in the breakup region. The asymptotic form for breakup is sufficiently complicated that knowing it has yet to provide a viable path to a first-principles calculation of the complete wave function.

We have devised a method that avoids this problem completely (*14*, *15*). We divided the problem into two steps: (i) computing the full wave function without explicit reference to any asymptotic form and (ii) extracting the required dynamical information from the computed wave function, again without explicit reference to an asymptotic form.

Computing the Wave Function for the Breakup Problem

To compute the wave function, we use a mathematical transformation of the Schrödinger equation itself that makes the wave function approach zero as the coordinates of any electron, $\mathbf{r}_i$, become large, just as it would in a bound state. Expressing the wave function as the sum of two terms, the scattered wave function, $\Psi_{sc}(\mathbf{r}_1,\mathbf{r}_2)$, plus the known initial state, $\Phi_o(\mathbf{r}_1,\mathbf{r}_2)$, allows us to rewrite the Schrödinger equation as

$$\begin{aligned}[E - H(\mathbf{r}_1,\mathbf{r}_2)]\Psi_{sc}(\mathbf{r}_1,\mathbf{r}_2) &= [H(\mathbf{r}_1,\mathbf{r}_2) - \mathrm{E}]\Phi_o(\mathbf{r}_1,\mathbf{r}_2) \\ &= [H(\mathbf{r}_1,\mathbf{r}_2) - E][\varphi_{1s}(\mathbf{r}_1)e^{i\mathbf{k}_i\cdot\mathbf{r}_2} \\ &\pm \varphi_{1s}(\mathbf{r}_2)e^{i\mathbf{k}_i\cdot\mathbf{r}_1}] \qquad (2)\end{aligned}$$

The electron coordinates are measured from the nucleus, and Φ_o describes the initial state of the system, namely, a free electron with momentum $\mathbf{k}_i$ incident on a hydrogen atom in its ground state, φ_{1s}. The $\pm$ sign determines the symmetry of the wave function under interchange of the coordinates $\mathbf{r}_1$ and $\mathbf{r}_2$, which is a consequence of the quantum mechanical indistinguishability of the electrons. The plus and minus signs depend on the total spin S of the two electrons: plus for singlets ($S = 0$) and minus for triplets ($S = 1$). The key aspect of Eq. 2 is that the scattered part of the wave function, $\Psi_{sc}(\mathbf{r}_1,\mathbf{r}_2)$, contains only outgoing waves at large distances and carries all of the information about the scattering dynamics.

The transformation we apply to the Schrödinger equation is called exterior complex scaling, under which a real scalar distance, r, is transformed as

$$R(r) = \begin{cases} r, & r < R_0 \\ R_0 + (r - R_0)e^{i\eta}, & r \geq R_0 \end{cases} \qquad (3)$$

where R_0 is a large real number and η is a positive number between 0 and π. This transformation is applied to the radial coordinates of both electrons. Exterior complex scaling of coordinates was invented by Simon (*16*) in 1979 to prove formal mathematical theorems in scattering theory (*17*). The crucial aspect of this transformation is that the scattered wave tends to zero exponentially at large distances because it is purely outgoing. Although a solution of the original Schrödinger equation in the breakup region would require the imposition of the complicated three-body asymptotic boundary condition, the transformed Schrödinger equation can be solved for the scattered wave by imposing the boundary condition that it vanish as either electron coordinate goes to infinity, exactly as though it were a bound state.

A pictorial representation of the exterior scaling transformation and its application in two dimensions is shown in Fig. 1. In the unshaded portion of the diagram, the electron coordinates r_1 and r_2 are both real. Thus, in this restricted region, the wave function we compute under the exterior scaling transformation coincides with the physical wave function for the system; that is, it is identical to the one that would be obtained by applying the correct Coulomb asymptotic boundary conditions for breakup.

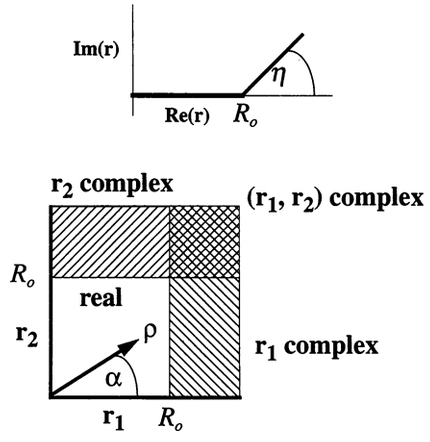

Fig. 1. The exterior complex scaling transformation. This mapping is applied to the radial coordinates of each electron. (**Top**) Real (Re) and imaginary (Im) parts of one radial coordinate plotted in the complex plane. The coordinate is real from 0 to R_0; beyond R_0, it is rotated into the upper half plane by an angle η. (**Bottom**) The scaling of a two-dimensional coordinate system. Both coordinates are real on an interior box extending from 0 to R_0. Outside of this box, at least one of the coordinates is complex. The hyperspherical coordinates ρ and α, which are used for calculating ionization flux, are also shown.

The Schrödinger equation for this problem is an equation in six variables. The next step to solving it is to expand the wave function in terms of functions of the angular coordinates of the electrons:

$$\Psi_{sc}(\mathbf{r}_1,\mathbf{r}_2) = \frac{1}{r_1 r_2} \sum_{L,l_1,l_2} \psi^L_{l_1 l_2}(r_1,r_2)\mathcal{Y}^L_{l_1 l_2}(\hat{\mathbf{r}}_1,\hat{\mathbf{r}}_2) \quad (4)$$

The functions $\mathcal{Y}^L_{l_1 l_2}$, so-called coupled spherical harmonics (*18*), are eigenfunctions of the total angular momentum, L, and the angular momenta of the individual electrons, l_1 and l_2. The use of the expansion given by Eq. 4 in the equation for the scattered wave results in sets of coupled two-dimensional second-order differential equations for the radial components of the wave function, $\psi^L_{l_1 l_2}(r_1,r_2)$. Because the total angular momentum is conserved, there is only coupling between components that have the same value of L.

We solve the resulting equations by converting them into large systems of complex linear equations using a finite difference representation of the Hamiltonian operator on a two-dimensional numerical grid. The grids used here, whose real portion extends out to 130 Bohr radii, consist of ~250,000 total points. The systems of complex linear equations that we solve are on the order of 5 million by 5 million. Such calculations require special techniques and are only practical to carry out on massively parallel supercomputers.

We can get a striking visualization of the scattering process by looking at the radial components of the scattered wave function. Three different radial components for $L = 2$ at an incident energy of 17.6 electron volts (eV) are shown in Fig. 2. The singlet component with $l_1 = l_2 = 1$ (Fig. 2A) is the easiest to explain. It is symmetric under interchange of r_1 and r_2. The large-amplitude oscillations along the r_1 and r_2 axes are due to discrete excitation processes in which one electron is confined to a region near the nucleus. The circular wavefronts that span the space between the two axes are due to ionization in which both electrons are moving away from the nucleus, and they exhibit the wavelength corresponding to the total energy available to the two outgoing electrons. The triplet component with $l_1 = l_2 = 1$ is shown in Fig. 2B. In contrast to the singlet component, this radial function is antisymmetric under the interchange of radial coordinates so the ionization wave is zero along the line $r_1 = r_2$. A component with $l_1 = 2$ and $l_2 = 0$ is shown in Fig. 2C. This component itself is

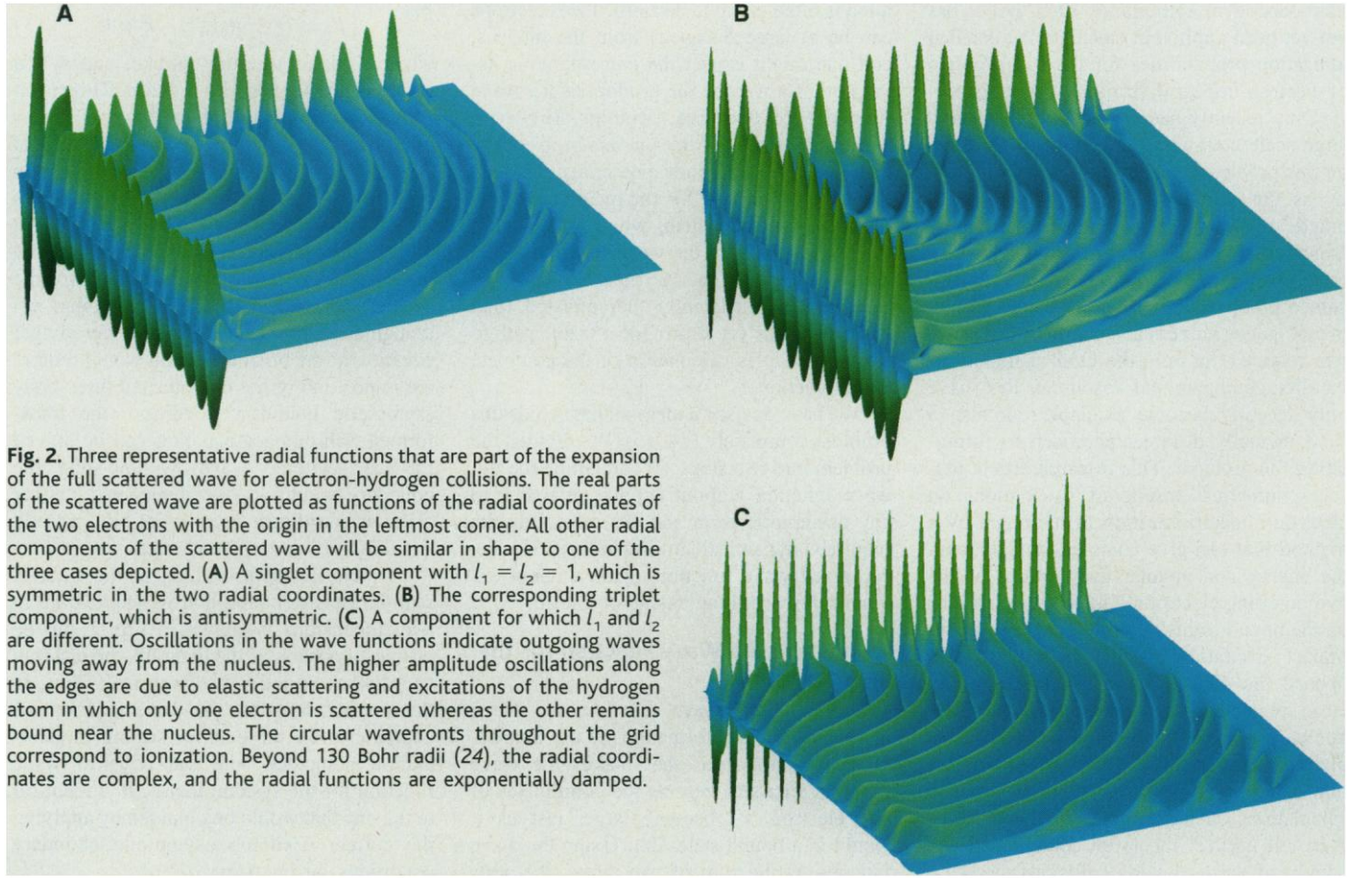

Fig. 2. Three representative radial functions that are part of the expansion of the full scattered wave for electron-hydrogen collisions. The real parts of the scattered wave are plotted as functions of the radial coordinates of the two electrons with the origin in the leftmost corner. All other radial components of the scattered wave will be similar in shape to one of the three cases depicted. (**A**) A singlet component with $l_1 = l_2 = 1$, which is symmetric in the two radial coordinates. (**B**) The corresponding triplet component, which is antisymmetric. (**C**) A component for which l_1 and l_2 are different. Oscillations in the wave functions indicate outgoing waves moving away from the nucleus. The higher amplitude oscillations along the edges are due to elastic scattering and excitations of the hydrogen atom in which only one electron is scattered whereas the other remains bound near the nucleus. The circular wavefronts throughout the grid correspond to ionization. Beyond 130 Bohr radii (*24*), the radial coordinates are complex, and the radial functions are exponentially damped.

asymmetric, but there is also a complementary component with $l_1 = 0$ and $l_2 = 2$ that preserves the overall symmetry of the full wave function. The large-amplitude, short-wavelength oscillations along the r_1 axis are due to elastic scattering. Longer wavelength processes that correspond to various excitations of the hydrogen atom are also present and cause the "beat" pattern in the amplitude near the r_1 axis. All of the radial components combine with the known angular factors to form the complete scattered wave through Eq. 4. Once the wave function is computed, we have information about all the physical processes that occur in this collision, but we must devise a way of extracting that information without recourse to the three-body asymptotic form.

Analyzing the Scattered Wave to Obtain Probabilities

Exterior complex scaling gives us a method for computing the physically correct wave function over a finite region of space where both r_1 and r_2 are real. The next task is to devise a method for analyzing this wave function to get probabilities and angular distributions for ionization. We do this by computing the quantum mechanical flux. The quantum mechanical flux is a concept dating from the 1920s on which formal scattering theory and the concept of scattering cross sections are based (*19*). For a two-electron system, the flux (or probability current density) is a six-dimensional vector defined as

$$\mathbf{F} = \frac{1}{2i}[(\Psi)^*\nabla\Psi - \Psi\nabla(\Psi)^*] \qquad (5)$$

where the asterisk denotes complex conjugation. The flux corresponding to ionization is evident in the outgoing waves seen in the radial functions plotted in Fig. 2. We want to describe the outgoing flux in a convenient coordinate system, hyperspherical coordinates, which replaces the two radial distances

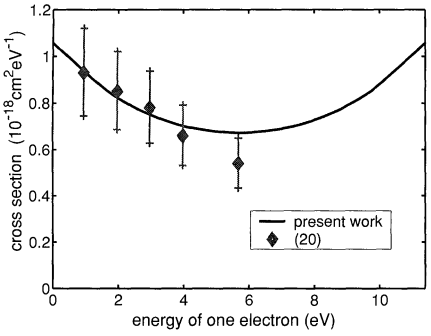

Fig. 3. Single differential ionization cross section (SDCS) for electron-hydrogen collisions at 25-eV incident energy. The ionization potential of hydrogen is 13.6 eV, so the total energy available to the ionized electrons is $E = 11.4$ eV. The calculated SDCS is symmetric about $E/2 = 5.7$ eV as expected. Experimental data from Shyn (*20*) are shown for comparison.

r_1 and r_2 by a hyperradius $\rho = (r_1^2 + r_2^2)^{1/2}$ and an angle $\alpha = \tan^{-1}(r_1/r_2)$ (see Fig. 1). As the electrons get very far apart, the angle α also parameterizes the energy sharing between the two electrons as $\varepsilon_1 = E\cos^2\alpha$ and $\varepsilon_2 = E\sin^2\alpha$. We can then label the outgoing flux at any point by $\mathbf{F}(\rho, \alpha, \theta_1, \varphi_1, \theta_2, \varphi_2)$. In the limit $\rho \to \infty$, this flux is directly proportional to the probability of ionization with electrons ejected with energies ε_1 and ε_2 and directions specified by the respective angles θ_1, φ_1, θ_2, and φ_2.

The wave function computed under exterior complex scaling is physically meaningful only in the region where both coordinates are real. Therefore, we must evaluate the flux through a hypersphere whose radius ρ lies within the unshaded portion of the grid shown in the lower portion of Fig. 1. It can be shown that, for electron-impact ionization, the probability computed in this fashion approaches its asymptotic limit as $1/\rho$. We obtain the $\rho \to \infty$ limit of the flux by extrapolating calculations performed for several sizes of the real part of the grid, R_0. We found that the flux reaches its asymptotic value quite smoothly for values of α that are not close to 0 or $\pi/2$. For the calculations reported here, the largest value of R_0 considered was 130 Bohr radii.

The Ionization Probabilities and Cross Sections

In scattering experiments, the probabilities for quantum events are usually expressed as a cross section with units of area, which for a particular process is the ratio of particles scattered per unit time to the flux (particles per unit time per unit area) of incident particles. For ionization, a number of different cross sections are frequently measured. The total cross section for ionization measures the total ionization probability at a given collision energy, irrespective of how the available energy is shared between the two free electrons that reach the detector or their direction of ejection relative to the incident beam. The single differential (SDCS) or energy-sharing cross section, $d\sigma/d\varepsilon$, measures the probability for ionization collisions that produce electrons at specific energies, irrespective of their directions of ejection. Because electrons are identical particles, it is physically impossible to distinguish which electron was originally bound in the atom. If ε_1 and ε_2 denote the energies of the two electrons in the final state (energy conservation demands that $\varepsilon_2 = E - \varepsilon_1$), then the SDCS must be symmetric about $E/2$. The SDCS is important because it plays a large part in determining the way energy is distributed among ions and electrons in low-temperature plasmas and in determining the electron energy distribution function itself. Unfortunately, experimental determination of the SDCS is difficult because it requires an extrapolation into regions where measurements are not possible (*20*).

The most detailed information about ionization is contained in the so-called triple differential cross section (TDCS), $d\sigma/(d\varepsilon d\Omega_1 d\Omega_2)$, which measures the ionization probability for producing electrons at specific energies and directions. The availability of such data places the most stringent test on the quality of a calculated wave function because it is sensitive to complex phases of its components.

We compute the SDCS by applying the flux operator to our calculated wave function. Integration over the directions of ejection of the two electrons, because of the orthonormality of the coupled spherical harmonics, collapses the SDCS expression into a simple sum of contributions from each radial component of the scattered wave function. Our calculated SDCS at an incident energy of 25 eV, along with the experimentally determined values of Shyn (*20*), is shown in Fig. 3. Other first-principles attempts to compute the SDCS have produced results that fail to display the proper symmetry about $E/2$ (*21*). Our results are symmetric about $E/2$, as they must be because they were extracted directly from a wave function with the proper exchange symmetry.

For the TDCS, there is no integration over the directions of ejection, and thus the cross section contains terms that depend on interference between the various partial wave components, $\psi^L_{l_1 l_2}(r_1, r_2)$, of the scattered wave function. The TDCS for electron-hydrogen ionization has been measured by Röder *et al.* (*22*, *23*) in the "symmetric coplanar" geometry. In this geometry, the electrons exit with the same energy, and the incident electron beam and the outgoing electrons all lie in the same plane. A diagram of the geometrical arrangement for this situation is shown in Fig. 4A. The experimentally determined values are plotted along with our calculated cross section in Fig. 4, B to F. Röder *et al.* (*23*) state that the absolute error for the experiments is as large as 40% but that the relative error is on the order of the sizes of the symbols. The small asymmetry about 90° in Fig. 4B suggests the size of the relative error, whereas the error bars show the absolute error.

Figure 4B describes the case in which the two detectors are placed 180° apart. The cross section in this case is strongly peaked at angles of 0° and 180°, where one electron is scattered forward and the other "recoils" in the backward direction. In the "symmetric coplanar" geometry, there is near zero probability of both electrons being ejected perpendicular to the direction of the incident electron. In the other cases depicted in Fig. 4, for which the detectors are separated by smaller angles, the lowest probabilities always correspond to the two electrons being scattered at equal but opposite angles from the incident direction. We verified that the curves shown in Fig. 4, B to E, are converged with respect to the number of angular momentum components included, whereas the larger discrepancy in Fig. 4F is due to the need for

more angular momentum components in our calculations to describe the ejection of electrons in closer directions. Overall, our results are in excellent agreement with measured values, both in shape and magnitude.

Understanding Ionizing Collisions and Their Role in Common Phenomena

The theoretical approach and numerical calculations we have presented here make possible a complete numerical solution of the simplest nontrivial problem in atomic collision theory—electron–hydrogen atom scattering—some 40 years after it was first attacked. The key to success in this work is the use of mathematical transformations that were originally invented as tools to prove formal theorems in mathematical physics and that avoid the explicit use of the asymptotic boundary condition for breakup that has been the barrier to such calculations for four decades. Although the calculations presented here will certainly be improved upon, their real importance is that the only approximations in the method are in the finite size of the grid that is used and the number of angular components retained in the expansion. The procedure we have outlined involves no uncontrolled approximations, and the effects of the numerical approximations can in principle be made arbitrarily small, given sufficient computing power. This fact distinguishes this approach from other theoretical methods that have been proposed to study ionization. Some have been found to give surprisingly good results, but, thus far, all have involved uncontrolled approximations that cannot be systematically eliminated.

Because low-energy electron-impact ionization pervades a wide range of physical processes, it is important to be able to predict the details of this most basic collision phenomenon in more complicated contexts. We have succeeded in solving the problem of electron-impact ionization of hydrogen, but further work needs to be done to treat ionization of many-electron atoms and molecules. Phenomena can appear that are absent from the two-electron system we treated here. With multielectron targets, there is the possibility of quantum interference between direct ionization and ionization from metastable states that may lead to signatures in the angular and energy distributions of exiting electrons. In the case of molecules, the additional nuclear degrees of freedom open the door to a richer set of phenomena such as fragmentation and attachment.

We expect that the ideas presented here will lead to further developments that will enable the treatment of ionizing collisions of electrons with more complicated atoms and molecules. There are several promising methods being developed within the electron-scattering theory community, and the ultimate solution to theoretical treatment of electron-impact ionization of molecules will undoubtedly draw on methods and concepts from several of these efforts. At a time when large-scale computers are generally thought to be necessary to investigate the "complexity" of the physical world in the very different sense of treating increasingly larger systems, it is noteworthy that the same computing power and tools are needed to answer a basic physics question for one of the simplest systems imaginable in physics and chemistry.

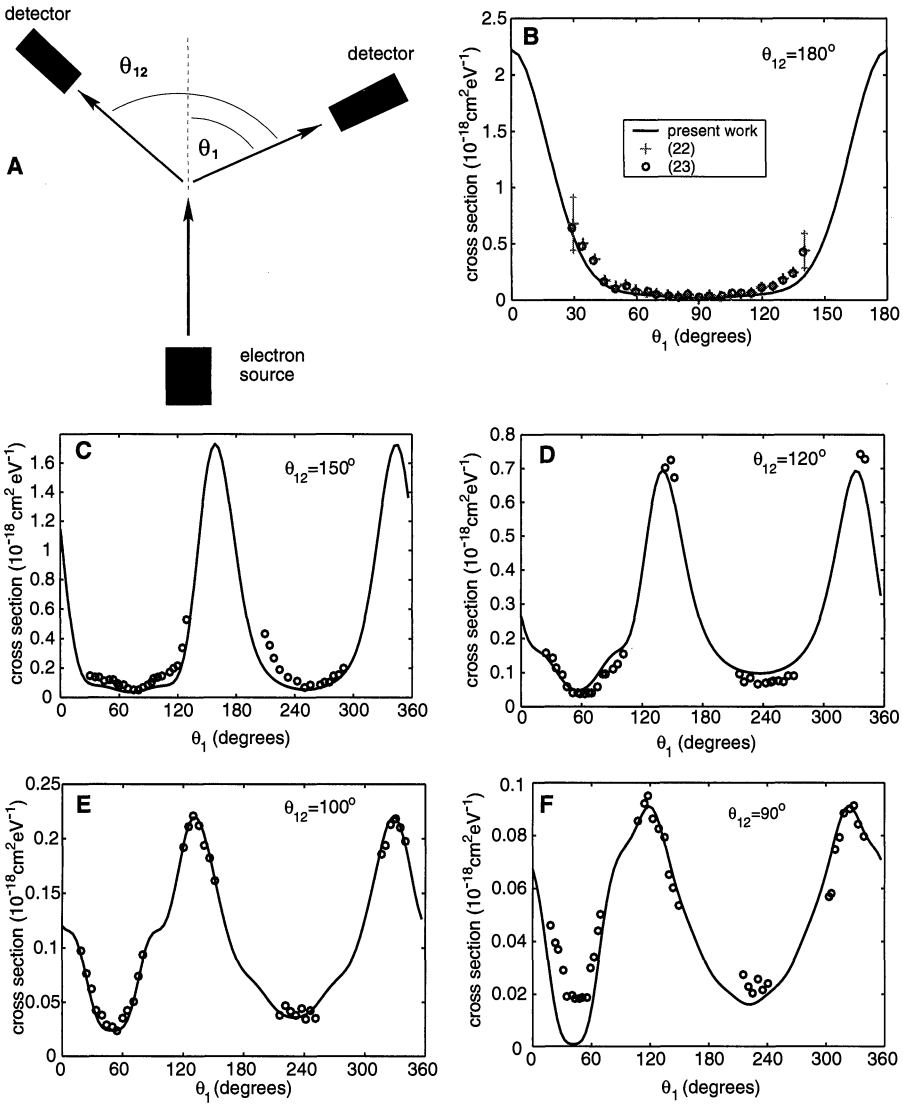

Fig. 4. (**A**) Geometrical arrangement for the equal energy-sharing, coplanar, triple differential cross sections (TDCSs) shown. The two detectors are tuned to measure electrons with half of the total energy. The detectors, electron source, and interaction region all lie in the same plane. (**B** to **F**) TDCSs at equal energy sharing for 17.6-eV incident energy. The plots presented correspond to both detectors being simultaneously rotated about the interaction region with the angle θ_{12} between them fixed. Experimental data of Röder *et al.* (*22*, *23*) are shown for comparison. The 1996 data (*22*) shown in each plot are from relative measurements and were originally given in a consistent, but undetermined set of units. The 1997 data (*23*) are from an absolute measurement but are available only for $\theta_{12} = 180°$. We compared the 1997 data with the corresponding 1996 data (B) to convert all of the 1996 values to an absolute scale. The statistical errors in the absolute measurements (*23*) are indicated for the leftmost and rightmost data points in (B).

References and Notes

1. E. A. Hylleraas, *Z. Phys.* **54**, 347 (1929).
2. C. L. Pekeris, *Phys. Rev.* **112**, 1649 (1958).
3. C. Schwartz, *Phys. Rev.* **124**, 1468 (1961).
4. W. Kohn, *Phys. Rev.* **74**, 1763 (1948).
5. P. G. Burke and K. Smith, *Rev. Mod. Phys.* **34**, 458 (1962).
6. I. Bray and A. T. Stelbovics, *Phys. Rev. Lett.* **70**, 746 (1993).
7. M. Baertschy, T. N. Rescigno, W. A. Isaacs, C. W. McCurdy, *Phys. Rev. A* **60**, R13 (1999).
8. J. Röder, H. Ehrhardt, I. Bray, D. V. Fursa, *J. Phys. B* **30**, 1309 (1997).
9. R. K. Peterkop, *Opt. Spectrosc.* **13**, 87 (1962); *Bull. Acad. Sci. USSR Phys. Ser.* **27**, 987 (1963).
10. M. R. H. Rudge and M. J. Seaton, *Proc. R. Soc. London Ser. A* **283**, 262 (1965).
11. M. Brauner, J. S. Briggs, H. Klar, *J. Phys. B* **22**, 2265 (1989).

12. S. P. Lucey, J. Rasch, C. T. Whelan, *Proc. R. Soc. London Ser. A* **455**, 349 (1999).
13. M. S. Pindzola and F. Robicheaux, *Phys. Rev. A* **55**, 4617 (1997); *Phys. Rev. A* **54**, 2142 (1996).
14. C. W. McCurdy, T. N. Rescigno, D. Byrum, *Phys. Rev. A* **56**, 1958 (1997).
15. C. W. McCurdy and T. N. Rescigno, *Phys. Rev. A* **56**, R4369 (1997).
16. B. Simon, *Phys. Lett. A* **71**, 211 (1979).
17. E. Balshev and J. M. Combes, *Commun. Math. Phys.* **22**, 280 (1971); B. Simon, *Commun. Math. Phys.* **27**, 1 (1972).
18. I. C. Percival and M. J. Seaton, *Proc. Cambridge Philos. Soc.* **53**, 654 (1957).
19. See, for example, L. I. Schiff, *Quantum Mechanics* (McGraw-Hill, New York, ed. 3, 1968).
20. T. W. Shyn, *Phys. Rev. A* **45**, 2951 (1992).
21. T. N. Rescigno, C. W. McCurdy, W. A. Isaacs, M. Baertschy, *Phys. Rev. A*, in press.
22. J. Röder *et al.*, *Phys. Rev. A* **53**, 225 (1996).
23. J. Röder *et al.*, *Phys. Rev. Lett.* **79**, 1666 (1997).
24. One Bohr radius is equal to 5.29×10^{-11} meters and one electron volt is equal to 1.60×10^{-19} joules.
25. This work was performed under the auspices of the U.S. Department of Energy by the Lawrence Livermore National Laboratory (LLNL) and the Lawrence Berkeley National Laboratory under contract numbers W-7405-Eng-48 and DE-AC03-76SF00098, respectively. The calculations were performed on the SGI/Cray T3E computer at the National Energy Research Scientific Computing Center (NERSC) and the IBM Blue-Pacific computer at LLNL. We thank X. Li at NERSC for providing us with her parallel LU factorization libraries for complex sparse matrices.

10 August 1999; accepted 21 September 1999

REPORTS

Quantum Impurity in a Nearly Critical Two-Dimensional Antiferromagnet

Subir Sachdev,* Chiranjeeb Buragohain, Matthias Vojta

The spin dynamics of an arbitrary localized impurity in an insulating two-dimensional antiferromagnet, across the host transition from a paramagnet with a spin gap to a Néel state, is described. The impurity spin susceptibility has a Curie-like divergence at the quantum-critical coupling, but with a universal effective spin that is neither an integer nor a half-odd integer. In the Néel state, the transverse impurity susceptibility is a universal number divided by the host spin stiffness (which determines the energy cost to slow twists in the orientation of the Néel order). These and numerous other results for the thermodynamics, Knight shift, and magnon damping have important applications in experiments on layered transition metal oxides.

The recent growth in the study of quasi–two-dimensional transition metal oxide compounds (*1*) with a paramagnetic ground state and an energy gap to all excitations with a nonzero spin (the "spin-gap" compounds such as $SrCu_2O_3$, $CuGeO_3$, and NaV_2O_5) has led to fundamental advances in our understanding of low-dimensional, strongly correlated electronic systems. These systems are insulators and thus are not as complicated as the cuprate high-temperature superconductors (which display a plethora of phases with competing magnetic, charge, and superconducting orders); this simplicity has exposed the novel characteristics of the collective quantum spin dynamics.

One of the most elegant probes of these spin-gap compounds is their response to intentional doping by nonmagnetic impurities, such as Zn or Li, at the location of the magnetic ions. Such experiments were initially undertaken on the cuprate superconductors (*2, 3*), but their analogs in the insulating spin-gap compounds have proved to be a fruitful line of investigation (*4*). They have demonstrated a remarkable property of the paramagnetic ground state of the host compound: Each nonmagnetic impurity has a net magnetic moment of spin ½ located in its vicinity (for the case in which the host compound has magnetic ions with spin ½). The confinement of spin is a fundamental defining property of the host paramagnet and is a key characterization of the quantum-coherent manner in which the host spins form a many-body, spin zero ground state; this confining property was predicted theoretically (*2, 5*) for the paramagnetic states of a large class of two-dimensional antiferromagnets.

We describe here the quantum theory of an arbitrary localized deformation in such antiferromagnets; examples of deformations are (i) a single nonmagnetic impurity, along with changes in the values of nearby exchange interactions, and (ii) a change in sign of a localized group of exchange interactions from antiferromagnetic to ferromagnetic. Our main concern is the behavior of the impurity as the host antiferromagnet undergoes a bulk quantum phase transition from a paramagnet to a magnetically ordered Néel state; we show that the spin dynamics of any deformation is universally determined by a single number—an integer or half-odd integer valued spin S.

Apart from applications to experiments on materials intentionally driven across a quantum phase transition, our results also lead to new insights and predictions about the behavior of impurities in existing spin-gap compounds. The traditional view of the spin-gap paramagnet is based on strong local singlet formation between nearest-neighbor spins (Fig. 1A); the resulting picture of doping by a nonmagnetic impurity is that the partner spin of the impurity site is essentially free. To obtain any nontrivial dynamics, one performs an expansion about such a decoupled limit, and this yields simple localized spin behavior with nonuniversal details, depending on the specific microscopic couplings. In practice, however, spin-gap systems are usually well away from the local singlet regime, and strong resonance between different singlet pairings leads to appreciable spin correlation lengths: Their spin gap, Δ, is significantly smaller than J, a typical nearest-neighbor exchange. A systematic and controlled approach for analyzing such a fluctuating singlet state, which we advocate here, is to find a quantum-critical point to a magnetically ordered state somewhere in parameter space and then to expand away from it into the spin-gap state. The coupling between the bulk and impurity excitations becomes universal in such an expansion, and all dynam-

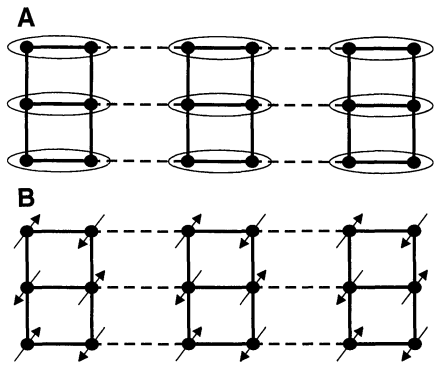

Fig. 1. The coupled-ladder antiferromagnet. The *A* links are solid lines and have exchange J; the *B* links are dashed lines and have exchange λJ. The paramagnetic ground state for $\lambda < \lambda_c$ is schematically indicated in (**A**): The ellipses represents a singlet valence bond, $(|\uparrow\downarrow\rangle - |\downarrow\uparrow\rangle)/\sqrt{2}$ between the spins on the sites. The Néel ground state for $\lambda > \lambda_c$ appears in (**B**).

Department of Physics, Yale University, Post Office Box 208120, New Haven, CT 06520–8120, USA.

*To whom correspondence should be addressed. E-mail: subir.sachdev@yale.edu